FIELD LAG EFFECTS ON THE VIBRATIONS OF ACTIVE MAGNETIC BEARING LEVITATED ROTORS

Chaesil Kim, A. B. Palazzolo, Punan Tang[1] and Daniel Manchala
Texas A&M University, College Station, Texas, U.S.A.

Albert Kascak[2], Gerald Brown, Gerald Montague[3]
NASA Lewis, Cleveland, Ohio, U.S.A.

Steve Klusman
Allison Engine Company, Indianapolis, Indiana, U.S.A.

ABSTRACT

The authors have developed sophisticated algorithms to predict the stability of active magnetic bearing (AMB) supported rotors. The rotor is modeled with finite elements while the feedback components-controller, power amplifier, actuators and sensors are given state space variable representations derived from their measured or predicted transfer functions. Correlation between test and theory has consistently shown an over prediction of active damping with both laminated and solid sleeve rotors. This paper shows the improvement in correlation achieved by including eddy current /hysteresis lag and rolloff effects in the simulation model.

INTRODUCTION

The vibrations of magnetic bearing supported or active vibration controlled rotors are affected by the stiffness, mass, damping and external force factors of conventional rotors plus the dynamics of the control-feedback components, i.e. sensors, controllers, power amplifiers and actuators. The coupled electro-mechanical system then governs critical speeds, unbalance response and stability. Simulation codes for conventional rotors lack the ability to incorporate the frequency dependent response characteristics of the feedback components. Hence a new simulation code was jointly developed by Texas A&M, NASA Lewis and U.S. Army for this purpose. In a previous paper Lin and Palazzolo, et al [1] demonstrated how transfer function representation of electrical components in feedback loop of control system could be accomplished by curve fitting the component's frequency response to that of a 2nd order low path electrical filter. This approach provided a 2nd order linear differential equation representation of the component which could be very easily coupled to the rotor system finite beam element model. They also provided solution of the characteristic equation of the closed loop system utilizing QR algorithm to extract the eigenvalues and to investigate stability. Maslen and Bielk [2] presented an approach for coupling a frequency dependent, feedback loop component with a generally defined transfer function, to a standard finite element rotor system model. This method avoids the problems encountered in transfer matrix based approaches to solve the closed loop stability problem, namely non-collocated sensor-actuators and frequency dependent feedback components. Tang and Palazzolo [3] presented a general methodology, coupling a F.E. based model of the rotor with state space models of the feedback control electromechanical components. This controller was applied to a cryogenic magnetic bearing test rig at NASA Lewis to predict the stability boundary and critical speeds, however only one

[1] Currently at Ream Corp., Fort Smith, Arkansas
[2] U.S. Army at NASA Lewis
[3] NYMA

transfer function for controller was employed. The current paper presents stability test and simulation results of a magnetic bearing supported gas turbine with a F.E. simulated B field transfer function (eddy current effect) and of a cryogenic magnetic bearing test rig at NASA Lewis with a measured B field/coil current transfer function. A closed loop electromechanical simulation approach is applied to the horizontal magnetic bearing gas turbine rig in figure 1. The transfer functions for the proportional path and the derivative path in the controller are modeled independently in the simulation. A nonlinear, magnetostatic field simulation for the horizontal magnetic bearing is employed in determining a stiffness for the magnetic control force/control current and the magnetic position stiffness due to bias current. These are compared to a static load/deflection experiment. A time harmonic magnetic field simulation for the magnetic bearing is employed for determining the frequency dependent field lag from eddy currents.

STATE SPACE REPRESENTATION OF FREQUENCY DEPENDENT FEEDBACK COMPONENTS

The electromechanical system contains feedback components which have frequency dependent characteristics such as the digital controller power amplifier and magnetic bearings (B field/coil current effect). The dynamic characteristics of the feedback electromechanical components can be represented in transfer function forms. These forms are obtained by curve fitting experimental/simulated data to complex rational functions. Tang [3] provided a curve fit methodology to obtain the transfer function from the frequency responses. The transfer functions have the general form;

$$\frac{V_{out}(s)}{V_{in}(s)} = G(s) = \frac{a_0 + a_1 s + a_2 s^2 + \ldots + a_{n-1} s^{n-1}}{b_0 + b_1 s + b_2 s^2 + \ldots + b_n s^n} \quad (1)$$

which are converted into the 1st order (time domain state-space) description;

$$\dot{V} = A_{n\times n} V + B_{n\times 1} V_{in}(t) \quad (2)$$

where

$$V_{out}(t) = C_{1\times n} V_{in}(t) \quad (3)$$

$$A_{n\times n} = \begin{bmatrix} 0 & 1 & 0 & \cdots & \cdots & 0 \\ 0 & 0 & 1 & 0 & \cdots & 0 \\ & & & \vdots & & \\ 0 & 0 & \cdots & \cdots & 0 & 1 \\ -\frac{b_0}{b_n} & -\frac{b_1}{b_n} & \cdots & \cdots & \cdots & -\frac{b_{n-1}}{b_n} \end{bmatrix} \quad (4)$$

and

$$B_{n\times 1} = \begin{pmatrix} 0 & 0 & \cdots & 0 & \frac{1}{b_n} \end{pmatrix}^T \quad (5)$$

where

$$C_{1\times n} = (a_0 \quad a_1 \quad \cdots \quad a_{n-1}) \quad (6)$$

$$V_{n\times 1} = \{V_1(t) \quad V_2(t) \quad \cdots \quad \cdots \quad V_{n-1}(t) \quad V_n(t)\}^T \quad (7)$$

Figure 2 through 3 show the comparison of the curve fit and measured frequency response functions for a unit gain proportional path through the PID hybrid controller and power amplifier. The agreement is seen to be excellent.

MAGNETIC FIELD SIMULATION FOR HORIZONTAL MAGNETIC BEARING

A magnetic field analysis for the gas turbine's homopolar horizontal magnetic bearing was performed to determine the current stiffness (control force/control current), the magnetic position stiffness and the frequency dependent field lag using a two dimensional finite element model.

The governing vector potential magnetic field equation is represented as;

$$\frac{1}{\mu} \nabla \cdot \nabla A = \sigma \frac{\partial A}{\partial t} - J_s \quad (8)$$

or

$$\frac{\partial}{\partial x}\left(\frac{1}{\mu}\frac{\partial A}{\partial x}\right) + \frac{\partial}{\partial y}\left(\frac{1}{\mu}\frac{\partial A}{\partial y}\right) = \sigma \frac{\partial A}{\partial t} - J_s \quad (9)$$

where J_s is source current density, σ is electric conductivity, μ is magnetic permeability and A is magnetic vector potential defined as $B = \nabla \times A$ where B is magnetic flux density.

For nonlinear magnetostatic field analysis eq. (9) is reduced to;

$$\frac{\partial}{\partial x}\left(\frac{1}{\mu}\frac{\partial A}{\partial x}\right)+\frac{\partial}{\partial y}\left(\frac{1}{\mu}\frac{\partial A}{\partial y}\right)=-J_s \qquad (10)$$

This equation is solved by employing a functional and enforcing the Dirichlet and Neumann boundary conditions. The functional is;

$$F(t)=\int_\Omega\left[\int_0^B \nu(B)\,B\,dB\right]d\Omega-\int_\Omega A\cdot J_s\,d\Omega \qquad (11)$$

where $\nu(B)$ is magnetic reluctivity ($=1/\mu_0\mu_r$)

The domain Ω is sub-divided into finite elements. In each element the solution is prescribed in terms of nodal values of the potential function, A. The functional is then minimized with respect to each of the nodal potentials. Due to the nonlinearity of magnetic permeability, a Newton iterative procedure is used to obtain the solution. The Maxwell stress tensor force calculation was employed in this analysis;

For two dimensional time harmonic field analysis the source current density is assumed to be time harmonic;

$$J_s=J_0 e^{j\omega t} \qquad (12)$$

and

$$A_s=A_0 e^{j\omega t} \qquad (13)$$

where J_0 is zero to peak amplitude of source current, A_0 is zero to peak amplitude of nodal vector potential and ω is angular frequency.

For this case equation (9) becomes;

$$\frac{\partial}{\partial x}\left(\frac{1}{\mu}\frac{\partial A_0}{\partial x}\right)+\frac{\partial}{\partial y}\left(\frac{1}{\mu}\frac{\partial A_0}{\partial y}\right)=j\omega\sigma A_0-J_0 \qquad (14)$$

Using the Galerkin method the governing integral equation is;

$$\int\{N\}^T\left[\frac{\partial}{\partial x}\left(\frac{1}{\mu}\frac{\partial A_0}{\partial x}\right)+\frac{\partial}{\partial y}\left(\frac{1}{\mu}\frac{\partial A_0}{\partial y}\right)-j\omega\sigma A_0+J_0\right]d\Omega=0 \qquad (15)$$

where $\{N\}$ is the shape function matrix.

The solution for the B field is obtained from;

$$B=\nabla\times A \qquad (16)$$

Figures 4(a) and 4(b) show the real and imaginary parts of the B field phasors at 50 Hz from the harmonic analysis. Note that the imaginary part has the opposite direction to those of the real parts indicating a lag

Figure 5 shows the results of harmonic analysis and curve fit transfer functions for applying both 100 % conductivity and 80 % conductivity in the rotor sleeve (solid Hiperco 27 material). Agreements between the simulated response and curve fit transfer functions are very good.

ASSEMBLY OF THE ROTOR SYSTEMS AND FEEDBACK COMPONENTS

The simulation code represents the rotor model with finite element (beams) and rigid inertias, while representing the feedback components with their measured or predicted transfer functions. The first order models of the feedback components are assembled with the rotor finite element model to form the coupled system model. Palazzolo [4] provides the n degree of freedom rotor bearing system equation in state space form as:

$$\begin{bmatrix} I & 0 \\ 0 & I \end{bmatrix}_{2n\times 2n}\begin{bmatrix}\ddot{X}\\ \dot{X}\end{bmatrix}+\begin{bmatrix} M^{-1}C & M^{-1}K \\ -I & 0\end{bmatrix}_{2n\times 2n}\begin{bmatrix}\dot{X}\\ X\end{bmatrix}=\begin{bmatrix} M^{-1}F(t)\\ 0\end{bmatrix}_{2n\times 1} \qquad (17)$$

The magnetic position stiffness was determined by considering both a static load/deflection test and magnetic field simulation.

The state space equation of the controller was divided into two parts, i.e. a proportional path and a derivative path:

$$\begin{bmatrix}\dot{V}_P\\ \dot{V}_D\end{bmatrix}=\begin{bmatrix} A_P & 0\\ 0 & A_D\end{bmatrix}\begin{bmatrix} X_P\\ X_D\end{bmatrix}+\begin{bmatrix} B_P\\ B_D\end{bmatrix}(V_C)_{in} \qquad (18)$$

and

$$(V_C)_{out}=\begin{bmatrix} K_P C_P & K_D C_D\end{bmatrix}\begin{bmatrix} X_P\\ X_D\end{bmatrix} \qquad (19)$$

Similarly, the power amplifier state space representation is:

$$\dot{V}_{PA}=A_{PA}X_{PA}+B_{PA}(V_{PA})_{in} \qquad (20)$$

and

$$(V_{PA})_{out}=C_{PA}X_{PA} \qquad (21)$$

The state space representation of the B field/coil current simulated transfer function (eddy current effect) is:

$$\dot{V}_E=A_E X_E+B_E(V_E)_{in} \qquad (22)$$

and

$$(V_E)_{out}=C_E X_E \qquad (23)$$

Since the magnetic bearing forces have been linearized with bias currents, the control forces are approximately proportional to the control currents:

$$F_{con} = \beta (V_E)_{in} P \tag{24}$$

where F_{con} represents the control force vector and P is the matrix ($n \times 1$) to locate the magnetic bearing force.

The current stiffness (Force/current), β was determined from the static load/deflection test and magnetic field simulation.

The input voltage to the controller is obtained as:

$$(V_C)_{in} = \xi\, G_{pr}\, T_{1\times n}\, X_{n\times 1} \tag{25}$$

where ξ is the probe sensitivity determined experimentally. G_{pr} is a signal amplifier gain and T is the matrix ($1\times n$) to locate the sensor.

The input voltage to the power amplifier and the coil current are;

$$(V_{PA})_{in} = (V_C)_{out} \tag{26}$$

$$I_{con} = (V_{PA})_{out} / R \tag{27}$$

where R is a resistance and I_{con} represents the control current in the coil. The input to the B/I transfer function is the coil current;

$$(V_E)_{in} = I_{con} \tag{28}$$

where V_E represents current instead of voltage.

Consider the free vibration case and assemble eqs. (17) through (28) to obtain the closed loop system equation;

$$[I]\{\dot{Z}\} + [Q]\{Z\} = 0 \tag{29}$$

where Q is dynamic matrix and Z is state space variable vector for closed loop AVC system;

$$\{Z\} = \begin{Bmatrix} \dot{X} \\ X \\ (X_p)_x \\ (X_D)_x \\ (X_{PA})_x \\ (X_E)_x \\ (X_p)_y \\ (X_D)_y \\ (X_{PA})_y \\ (X_E)_y \end{Bmatrix} \tag{30}$$

$$[Q] = [Q_1\ Q_2\ Q_3] \tag{31}$$

$$Q_1 = \begin{bmatrix} M^{-1}C & M^{-1}K & 0 & 0 \\ -I & 0 & 0 & 0 \\ 0 & -\xi_x G_{pr} B_P T_x & -A_P & 0 \\ 0 & -\xi_x G_{pr} B_D T_x & 0 & -A_D \\ 0 & 0 & -K_P B_{PA} C_P & -K_D B_{PA} C_P \\ 0 & 0 & 0 & 0 \\ 0 & -\xi_y G_{pr} B_P T_y & 0 & 0 \\ 0 & -\xi_y G_{pr} B_D T_y & 0 & 0 \\ 0 & 0 & 0 & 0 \\ 0 & 0 & 0 & 0 \end{bmatrix} \tag{32}$$

$$Q_2 = \begin{bmatrix} 0 & -\beta_x M^{-1} P_x C_E & 0 \\ 0 & 0 & 0 \\ 0 & 0 & 0 \\ 0 & 0 & 0 \\ -A_{PA} & 0 & 0 \\ -B_E C_{PA} / R & -A_E & 0 \\ 0 & 0 & -A_P \\ 0 & 0 & 0 \\ 0 & 0 & -K_P B_{PA} C_P \\ 0 & 0 & 0 \end{bmatrix} \tag{33}$$

$$Q_3 = \begin{bmatrix} 0 & 0 & -\beta_y M^{-1} P_y C_E \\ 0 & 0 & 0 \\ 0 & 0 & 0 \\ 0 & 0 & 0 \\ 0 & 0 & 0 \\ 0 & 0 & 0 \\ 0 & 0 & 0 \\ -A_D & 0 & 0 \\ -K_D B_{PA} C_D & -A_{PA} & 0 \\ 0 & -B_E C_{PA} / R & -A_E \end{bmatrix} \tag{34}$$

The eigensolutions for eq. (33) are obtained by substituting

$$Z = \Psi e^{\lambda t} \tag{35}$$

yielding

$$Q\Psi = -\lambda\Psi \tag{36}$$

The eigenvalues/eigenvectors are extracted from this equation utilizing the QR algorithm.

CLOSED LOOP STABILITY RESULTS

The zero-speed stability boundary was measured by lowering the derivative feedback gain K_D while maintaining a constant proportional feedback gain K_P and observing the shaft's vibration orbit on an oscilloscope. An abrupt increase in vibration indicated unstable operation by this method. The stability bound is extremely important since it defines the range in which the derivative and proportional feedback gains may be adjusted to provide desired active stiffness and damping.

The initial correlation for the gas turbine engine simulator was poor as shown in figure 7 (w/o eddy current curve). The apparent loss in derivative gain effectiveness for stabilizing the system could be explained by including effects of eddy currents set up on the non-laminated rotor sleeve or by material hysteresis. A time harmonic eddy current simulation was performed employing finite elements, which yielded a transfer function between the B field and the coil current. Figure 4 (a,b) show the real and imaginary parts of the B field phasors at a frequency of 50 Hz. A significant lag was predicted by the F.E. model which provided an explanation for the loss in active damping (derivative gain). The F.E. simulation was sensitive to the surface conductivity value for the rotor sleeve-flux conduction path. The result in figure 7 shows how the stability bound prediction improved significantly when the predicted B field/coil current transfer function was included and even closer agreement was achieved if 80 % of the nominal surface conductivity value was used in the eddy current F.E. simulation.

The NASA magnetic bearing test rig correlation between the predicted and measured bounds was significantly improved when the measured transfer function between the coil current and the bearing's B field was included in the model as shown in figure 8. The validity of the code was also confirmed in this case by comparing the measured and predicted unstable oscillation frequency at the instability boundary. Figure 9 shows very close agreement especially when the measured B field/coil current transfer function is inserted into the model (B/I include). Note that the instability frequency "jumps" from the first to the second mode at a proportional feedback gain of approximately K_P=3.

REFERENCES

[1] Lin, R. R., Palazzolo, A. B.,Kascak, A. F., Montague, G. T., 1991, " Electromechanical Simulation and Testing of Actively Controlled Rotordynamic Systems with Piezoelectric Actuators," presented at the International Gas Turbine Conference, Orlando, Florida, June 3-6, Accepted for publication in the Transactions of the ASME.

[2] Maslen, E. H. and Bielk, J. R., 1991, " Implementing Magnetic Bearing in Discrete Flexible Structure Modals," Submitted to Transaction of ASME *Journal of Dynamics and Controls.*

[3] Tang. P., Palazzolo, A. B., et al., 1994, "An Electromechanical Simulation Method For Active Vibration Control of a Magnetic Bearing Supported Rotor," ASME 1994 Gas Turbine Conference, ASME Paper 93-GT-382, Cincinnati, Ohio.

[4] Palazzolo, A.B., Wang, B. P., 1983, " Eigensolution Reanalysis of Rotor Dynamic System by the Generalized Receptance Method," Transaction of ASME *Journal of Engineering for Power,* Vol.105, pp. 543-550.

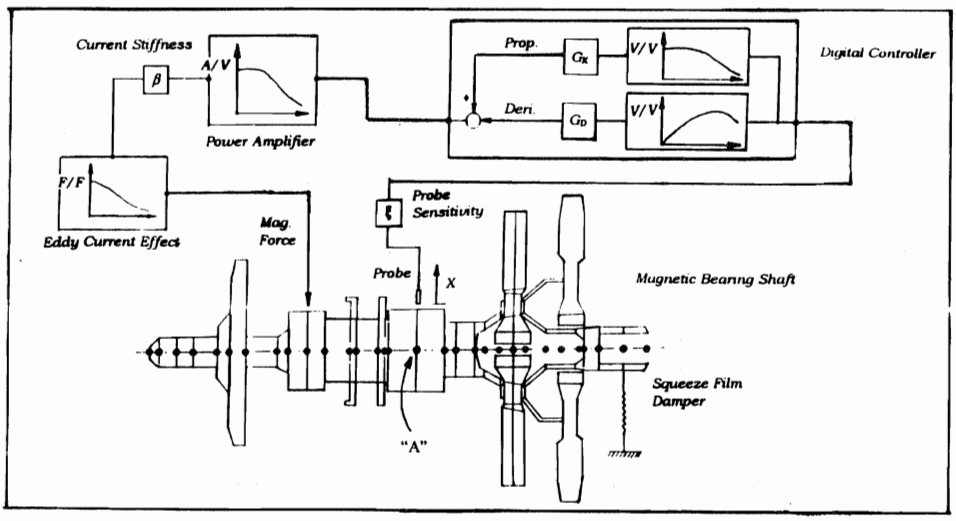

FIGURE 1. Gas Turbine Simulator Feedback Loop and Finite Element Model

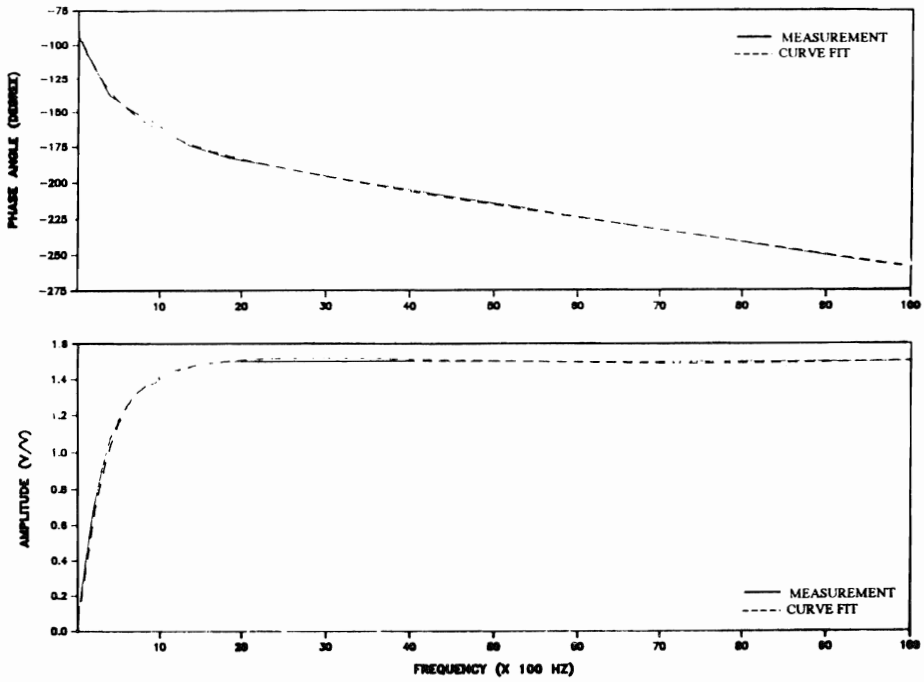

FIGURE 2. Transfer Function for PID Hybrid Controller (Derivative Path)

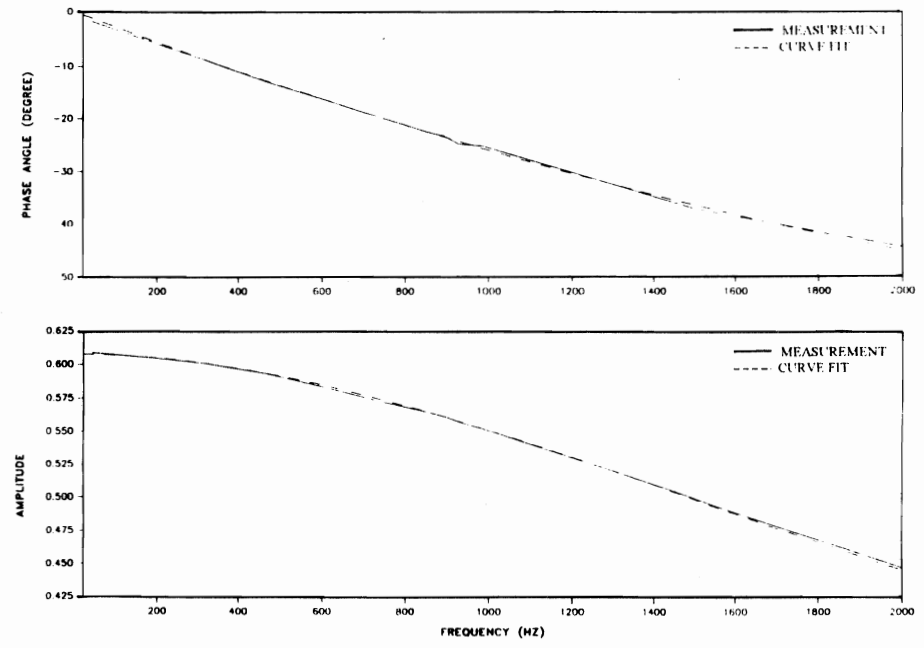

FIGURE 3. Transfer Function for Power Amplifier

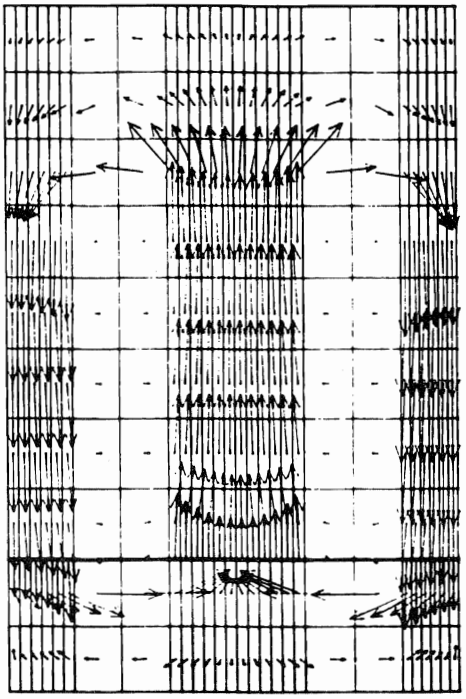

FIGURE 4 (a). Real Part of B Field Phasors at 50 Hz

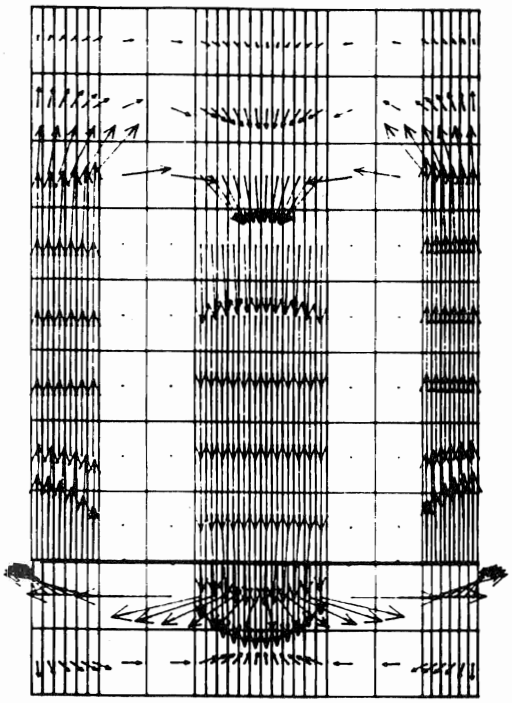

FIGURE 4 (b). Imaginary Part of B Field Phasors at 50 Hz

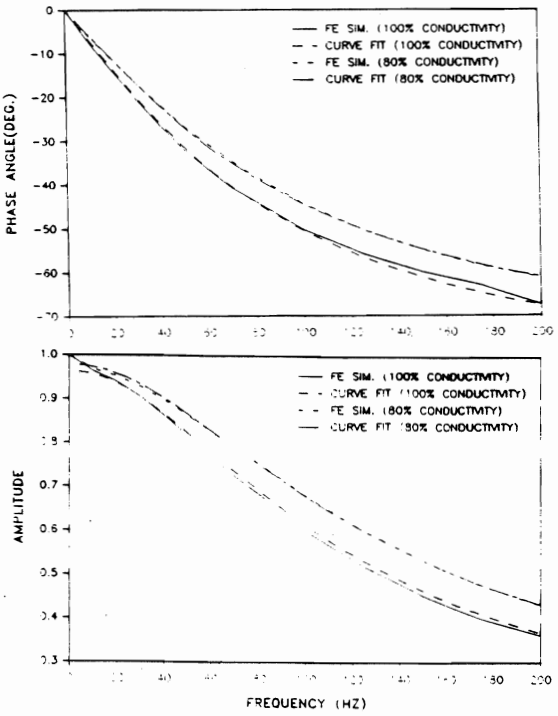

FIGURE 5. Transfer Function for B Field/Coil Current

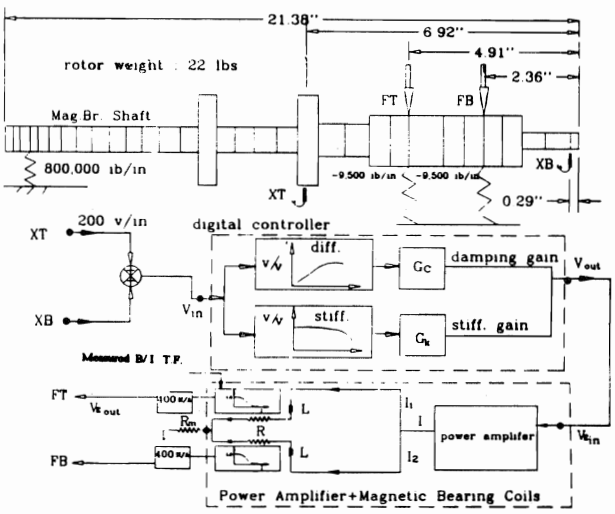

FIGURE 6. Block Diagram of Rotor, Controller and Cryogenic Magnetic Bearing

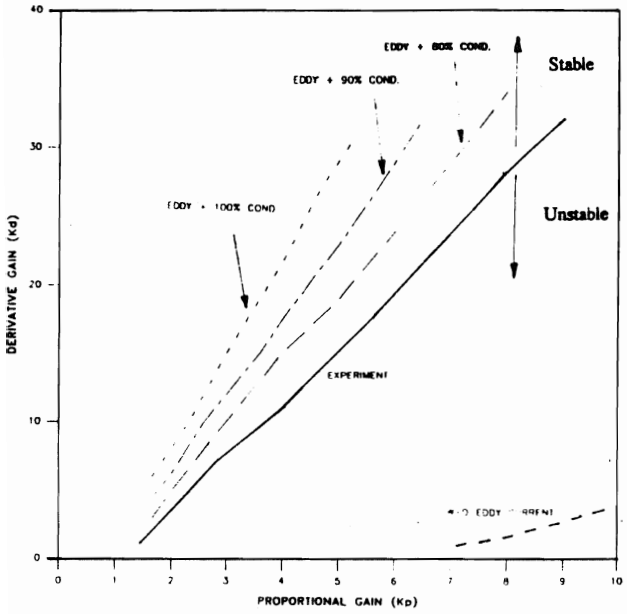

FIGURE 7. Measured and Predicted Stability Boundaries for Gas Turbine Engine Simulator

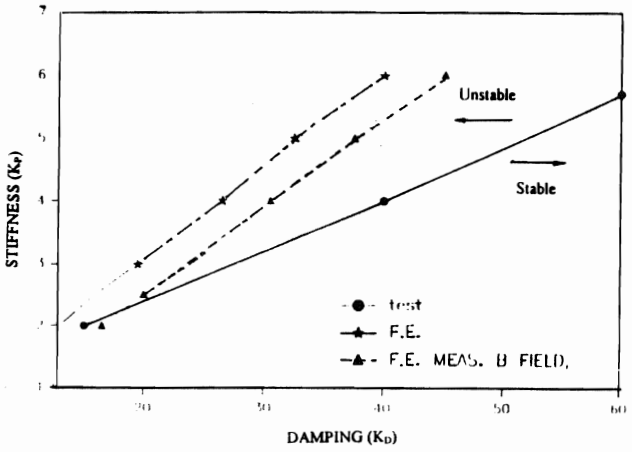

FIGURE 8. Comparison of Measured and Predicted Instability Boundary with Measured B Field Effects (Cryogenic Magnetic Bearing)

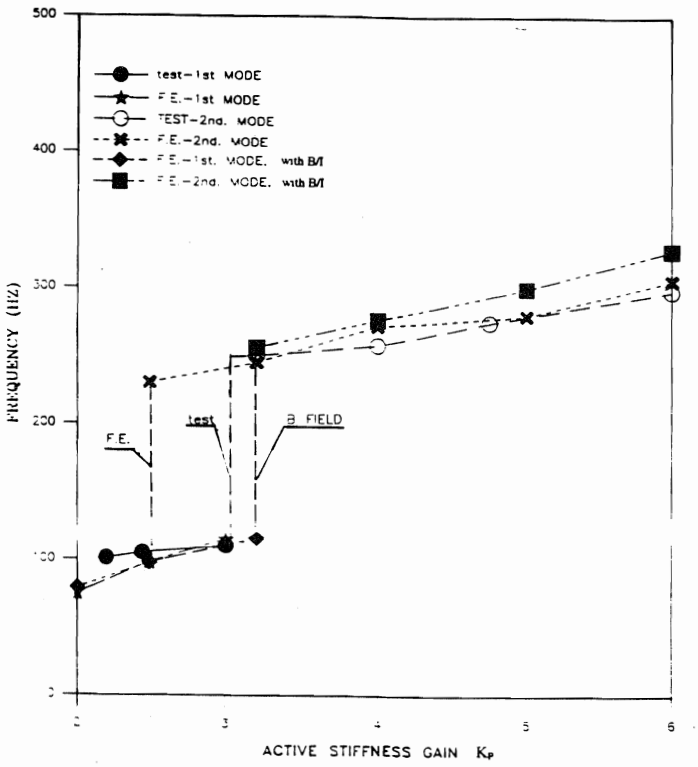

FIGURE 9. Comparison of Measured and Predicted Natural Frequencies at the Instability Threshold (Cryogenic Magnetic Bearing)